Inorg. Chem. **2003**, *42*, 7460–7471

Solid State Coordination Chemistry of Oxomolybdenum Organoarsonate Materials

Eric Burkholder,[†] Suzanne Wright,[†] Vladimir Golub,[‡] Charles J. O'Connor,[‡] and Jon Zubieta*,[†]

Departments of Chemistry, Syracuse University, Syracuse, New York 13244, and University of New Orleans, New Orleans, Louisiana 70148

Received May 23, 2003

The oxomolybdenum–arsonate system was investigated under hydrothermal conditions in the presence of charge-compensating copper(II)–organonitrogen complex cations as secondary building blocks. A series of materials of the Mo/O/As/Cu/ligand family has been prepared and structurally characterized. The architectures of the products reflect the identity of the arsonate component and the organonitrogen ligand, as well as the reaction conditions. The structural versatility of this emerging class of compounds is manifested by the one-dimensional structures of $[\{Cu(o\text{-phen})(H_2O)_2\}_2Mo_6O_{18}(O_3AsOH)_2]$ (**1**), $[\{Cu(terpy)\}_2Mo_4O_{13}H(AsO_4)_2]\cdot 2H_2O$ (**2**·2H$_2$O), $[\{Cu(2,2'\text{-bpy})(H_2O)\}_2\text{-}Mo_6O_{18}(O_3AsC_6H_5)_2]\cdot 2H_2O$ (**4**·2H$_2$O), and $[\{Cu(o\text{-phen})(H_2O)\}_2\{Mo_6O_{18}(O_3AsC_6H_5)_2\}]\cdot 4H_2O$ (**5**·4H$_2$O), by the two-dimensional materials $[\{Cu_2(tpyprz)(H_2O)_2\}Mo_6O_{18}(O_3AsOH)_2]\cdot 2H_2O$ (**3**·2H$_2$O), $[\{Cu(terpy)\}_2Mo_6O_{18}(O_3AsC_6H_5)_2]\cdot H_2O$ (**6**·H$_2$O), and $[\{Cu_2(tpyprz)\}Mo_6O_{18}(O_3AsC_6H_5)_2]\cdot 2H_2O$ (**7**·2H$_2$O), and the molecular clusters $[\{Cu(2,2'\text{-bpy})_2\}_2Mo_{12}O_{34}(O_3AsC_6H_5)_4]\cdot 2.35H_2O$ (**8**·2.35H$_2$O) and $[Cu(o\text{-phen})(H_2O)_3][Cu(o\text{-phen})_2Mo_{12}O_{34}(O_3AsC_6H_5)_4]\cdot 3H_2O$ (**9**·3H$_2$O).

Introduction

Hybrid materials combine the unique characteristics of their organic and inorganic components in a complementary fashion to provide novel solid state structures, exhibiting composite or even new properties.[1−9] The inorganic oxides provide several extensive families of materials which illustrate the profound structural consequences of the incorporation of organic substructures into the oxide architecture. These include nature's remarkable products of biomineralization,[10−12] as well as zeolites,[13,14] mesoporous oxides,[15,16] transition metal phosphates with entrained organic cations,[17] and the prototypical examples of hybrid materials, the metal organophosphonates.[18,19] This latter family of compounds characteristically exhibits a structure type of alternating organic and inorganic layers, either an M/O/P layer decorated on both surfaces by the organic component in the case of the simple $\{O_3PR\}^{2-}$ subunit (Scheme 1a) or M/O/P layers buttressed by organic tethers in the case of diphosphonate $\{O_3P(CH_2)_nPO_3\}^{4-}$ units (Scheme 1b).

Recently, we demonstrated a building block approach to the design of metal−organophosphonates which exploited well-defined clusters with a fixed number of directional bonding sites to determine the ultimate connectivity and dimensionality of these materials.[20−23] As shown in Scheme 2, the "venerable" polyoxomolybdates of the $[Mo_5O_{15}(O_3PR)_2]^{4-}$ family[24] provide building blocks for one-dimensional organic/

* To whom correspondence should be addressed. E-mail: jazubiet@syr.edu.
† Syracuse University.
‡ University of New Orleans.

(1) Hagrman, P. J.; Hagrman, D.; Zubieta, J. *Angew. Chem., Int. Ed.* **1999**, *38*, 2639.
(2) Braga, D.; Grepioni, F.; Desirajee, G. R. *Chem. Rev.* **1998**, *98*, 1375.
(3) Chen, B.; Eddaoudi, M.; Hyde, T. S.; O'Keefe, M.; Yaghi, O. M. *Science* **2001**, *291*, 1021.
(4) Kim, J.; Chen, B.; Reineke, T. M.; Li, H.; Eddaoudi, M.; Moler, D. B.; O'Keefe, M.; Yaghi, O. M. *J. Am. Chem. Soc.* **2001**, *123*, 8239.
(5) Vaidhyanathan, R.; Natarajan, S.; Rao, C. N. *Chem. Mater.* **2001**, *13*, 3524.
(6) Distler, A.; Sevov, S. C. *Chem. Commun.* **1998**, 959.
(7) Mitzi, D. B.; Dimitrakopoulos, C. D.; Korba, L. L. *Chem. Mater.* **2001**, *13*, 3728.
(8) Kanatzidis, M. G.; Dan, B. K. *Comments Inorg. Chem.* **1999**, *21*, 29.
(9) Guby, A. M.; Tang, Z.; Miranda, P. B.; Sidanov, V. I. *Adv. Mater.* **2001**, *13*, 833.
(10) Hench, L. L. Inorganic Biomaterials. In *Materials Chemistry, an Emerging Discipline*; Interrante, L. V., Casper, L. A., Ellis, A. B., Eds.; ACS Series 245; American Chemical Society: Washington, DC, 1995; Chapter 21, pp 523−547.
(11) Lowenstan, H. A.; Weiner, S. *On Biomineralization*; Oxford University Press: New York, 1989.
(12) Estroff, L. A.; Hamilton, A. D. *Chem. Mater.* **2001**, *13*, 3227.
(13) *Introduction to Zeolite Science and Practice*; van Bekkum, H., Flanigan, E. M., Jansen, J. C., Eds.; Elsevier: Amsterdam, 1991.
(14) Balkus, K. J. *Prog. Inorg. Chem.* **2001**, *50*, 217.
(15) Biz, S.; Occelli, M. L. *Catal. Rev. Sci. Eng.* **1998**, *40*, 329.
(16) Kresge, C. T.; Leonowicz, M. E.; Roth, W. J.; Vartuli, J. C.; Beck, J. S. *Nature* **1992**, *359*, 710.

10.1021/ic030171f CCC: $25.00
Published on Web 10/24/2003

Scheme 1

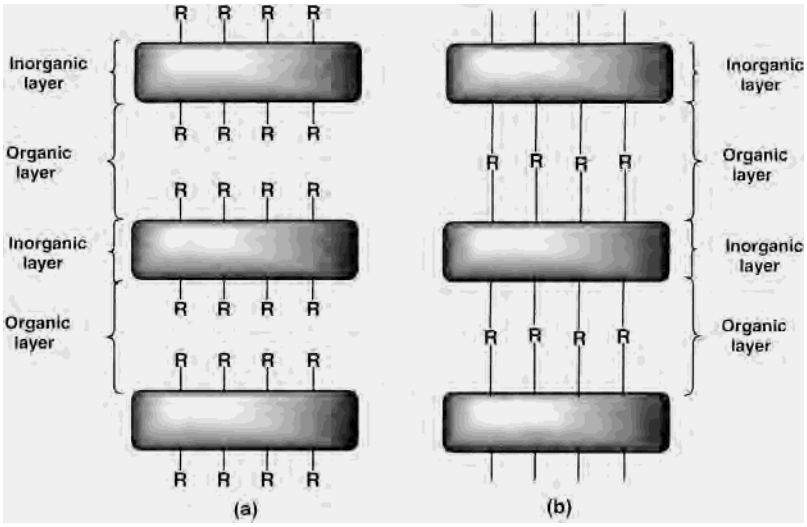

Scheme 2

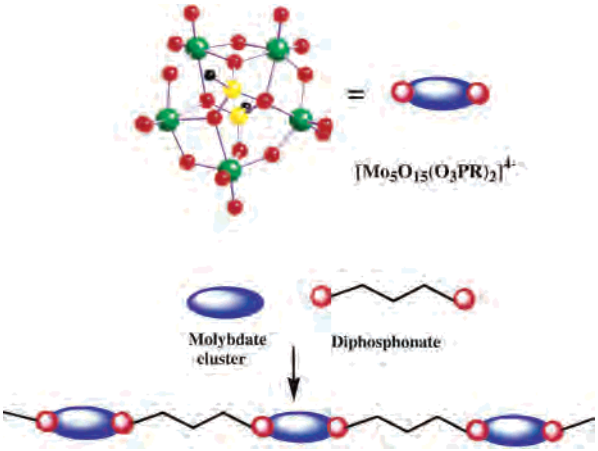

inorganic oxides through the tethering of the organophosphonate components with appropriate organic linkers. A noteworthy feature of the chemistry of these materials was the absolute requirement of a secondary metal/ligand subunit to provide charge compensation and to passivate the surface of the molybdate cluster to prevent expansion into the favored two-dimensional Mo/O/P structure under the hydrothermal synthesis condition. This observation led to the construction of two-dimensional phases by the simple expedient of introducing a binucleating ligand in the secondary metal/ligand subunit to allow expansion in the second dimension (Scheme 3).

Although there are now approximately 20 examples of such oxomolybdenum organodiphosphonate materials, it is noteworthy that the architectures are exclusively one- and two-dimensional. This observation reflects the simple construction principles outlined here, which in turn reflect the number of points of attachment available on the periphery of the $[Mo_5O_{15}(O_3PR)_2]_n^{4n-}$ clusters. The ring size and the steric requirements of the diphosphonate linkers limit the surface sites to three and prevent expansion in the third

(17) The chemistry of metal phosphate solids incorporating organic structure-directing components has been extensively studied in recent years. Representative publications include: (a) Haushalter, R. C.; Mundi, L. A. *Chem. Mater.* **1992**, *4*, 31. (b) Khan, M. I.; Meyer, L. M.; Haushalter, R. C.; Schweitzer, C. L.; Zubieta, J.; Dye, J. L. *Chem. Mater.* **1996**, *8*, 43. (c) Livage, C.; Millange, F.; Walter, R. I.; Loiseau, T.; Simon, N.; O'Hare, D.; Férey, G. *Chem. Commun.* **2001**, 994. (d) Do, J.; Bontchev, P.; Jacobson, A. J. *Chem. Mater.* **2001**, *13*, 2601. (e) Choudhury, A.; Natarajan, S.; Rao, C. N. R. *Inorg. Chem.* **2000**, *39*, 4295. (f) Liu, Y.; Shi, Z.; Zhang, L.; Fu, Y.; Chen, J.; Li, B.; Hua, J.; Pang, W. *Chem. Mater.* **2001**, *13*, 2017. (g) Zhou, Y.-S.; Zhang, L.-J.; You, X.-Z.; Natarajan, S. *J. Solid State Chem.* **2001**, *159*, 209. (h) Christensen, A. N.; Baregis, A.; Nielson, R. B.; Hazell, R. G.; Morley, P.; Hanson, J. C. *J. Chem. Soc., Dalton Trans.* **2001**, 1611. (i) Harrison, W. T. A.; Phillips, M. L. F.; Stanchfield, J.; Newoff, T. M. *Inorg. Chem.* **2001**, *40*, 895. (j) Chiang, R.-K. *Inorg. Chem.* **2000**, *39*, 4985. (k) Neeraj, S.; Natarajan, S. *Chem. Mater.* **2000**, *12*, 2753. (l) Chippendale, A. *Chem. Mater.* **2000**, *12*, 818. (m) Neeraj, S.; Natarajan, S.; Rao, C. N. R. *Angew. Chem., Int. Ed.* **1999**, *38*, 3480. (n) Huang, C.-H.; Huang, L.-H.; Lii, K. H. *Inorg. Chem.* **2001**, *40*, 2625.

(18) The chemistry of the metal organophosphonates has witnessed remarkable growth in the past decade. A number of useful reviews are available: (a) Clearfield, A. *Prog. Inorg. Chem.* **1998**, *47*, 371. (b) Alberti, G. In *Comprehensive Supramolecular Chemistry*; Atwood, J. L., Davis, J. E. D., Vogel, F., Eds.; Pergamon Press: New York, 1996; Vol. 9 (Alberti, G., Bein, T., Eds.), p 152. (c) Clearfield, A. In *Comprehensive Supramolecular Chemistry*; Atwood, J. L., Davies, J. E. D., Vogel, F., Eds.; Pergamon Press: New York: 1966; Vol. 9 (Alberti, G., Bein, T., Eds.), p 107. (d) Clearfield, A. *Chem. Mater.* **1998**, *10*, 2801. (e) Vermeulen, L. A. *Prog. Inorg. Chem.* **1997**, *44*, 143.

(19) In addition to work referenced in these reviews, a wealth of new information on metal−phosphonates has been published in the last two years. Some representative examples of novel results in this field include: (a) Clearfield, A.; Sharma, C. V. K.; Zhang, B. *Chem. Mater.* **2001**, *13*, 3099. (b) Barthelet, K.; Merlier, C.; Serre, C.; Riou-Cavellec, M.; Riou, D.; Férey, G. *J. Mater. Chem.* **2002**, *12*, 1132. (c) Trobajo, C.; Khaisalsov, S. A.; Espina, A.; Garcia, J. R. *Chem. Mater.* **2001**, *13*, 4457. (d) Yin, P.; Zhang, L.-M.; Gao, S.; Xin, X.-Q. *Chem. Commun.* **2001**, 2346. (e) Hix, G. B.; Kariuki, B. M.; Kitchin, S.; Tremayne, M. *Inorg. Chem.* **2001**, *40*, 1477. (f) Odolul, F.; Bujoli, B.; Massiot, D. *Chem. Mater.* **2001**, *13*, 163. (g) Adair, B. A.; deDelgado, G. D.; Delgado, J. M.; Cheetham, A. K. *Solid State Sci.* **2000**, *2*, 119. (h) Neeraj, S.; Forster, P. M.; Rao, C. N. R.; Cheetham, A. K. *Chem. Commun.* **2001**, 2716. (i) Bellitto, C. In *Magnetism: Molecules to Materials II*; Miller, J. S., Drilles, M., Eds.; 2001; p 425. (j) Vioux, A.; Mutin, P.; Le Bideau, J.; Leclercq, D. Organophosphorus-based organic−inorganic hybrids. *Mater. Res. Soc. Symp. Proc.* **2001**, 628 (Organic/Inorganic Hybrid Materials, CC1.4.1−CC1.4.12.).

(20) Finn, R. C.; Zubieta, J. *Inorg. Chem.* **2001**, *40*, 2466.

(21) Burkholder, E.; Zubieta, J. *Chem. Commun.* **2001**, 2056.

(22) Finn, R. C.; Burkholder, E.; Zubieta, J. *Chem. Commun.* **2001**, 1852.

(23) Finn, R. C.; Rarig, R. S.; Zubieta, J. *Inorg. Chem.* **2002**, *41*, 2109.

(24) Kwak, W.; Pope, M. T.; Scully, T. F. *J. Am. Chem. Soc.* **1975**, *97*, 5735.

Scheme 3

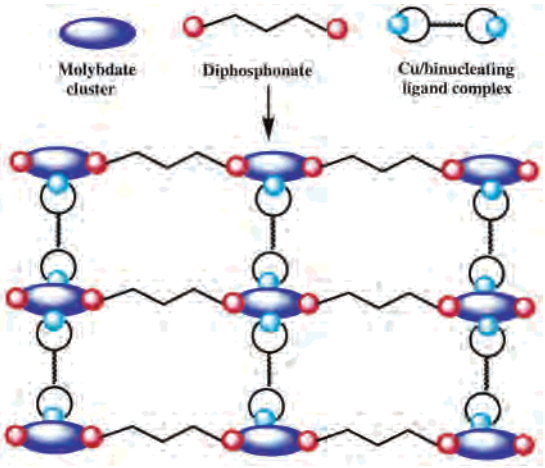

dimension. This observation naturally led to the consideration of larger building blocks with potential for expanded connectivity sites as synthons. The analogous oxomolybdenum organoarsonate clusters are also well-documented materials,[25,26] which as a consequence of the larger covalent radius of arsenic in comparison to that of phosphorus form hexanuclear rings $\{Mo_6O_{18}(O_3AsR)_2\}^{4-}$, in contrast to the pentanuclear rings of the phosphorus family. Since the architectures of such cluster based extended structures are determined not only by the dispositions of the potential points of attachment on the cluster surface but by the number of points of attachment as well, the ring size of the cluster synthon should influence the connectivity to the secondary metal−ligand substructure and consequently the pattern of expansion in one-, two or three-dimensions. This point is illustrated schematically in Scheme 4.

Herein, we report the syntheses and structural characterization of a series of Mo/O/AsR/Cu(II)−ligand phases, where AsR is $[O_3AsOH]^{2-}$ or $[O_3AsC_6H_5]^{2-}$ and ligand is *o*-phenanthroline, 2,2′:6′,2″-terpyridine, 2,2′-bipyridine, or tetra-2-pyridinylpyrazine. The remarkable structural versatility of this class of compounds is demonstrated by the one-dimensional structures of $[\{Cu(o\text{-phen})(H_2O)_2\}_2Mo_6O_{18}(O_3AsOH)_2]$(**1**), $[\{Cu(terpy)\}_2Mo_4O_{13}H(AsO_4)]_2\cdot 2H_2O$ (**2**·$2H_2O$), $[\{Cu(2,2'\text{-bpy})(H_2O)\}_2Mo_6O_{18}(O_3AsC_6H_5)_2]\cdot 2H_2O$ (**4**·$2H_2O$), and $[\{Cu(o\text{-phen})(H_2O)\}_2Mo_6O_{18}(O_3AsC_6H_5)_2]\cdot 4H_2O$ (**5**·$4H_2O$), by the two-dimensional materials $[\{Cu_2(tpyprz)(H_2O)_2\}Mo_6O_{18}(O_3AsOH)_2]\cdot 2H_2O$ (**3**·$2H_2O$), $[\{Cu(terpy)\}_2Mo_6O_{18}(O_3AsC_6H_5)_2]\cdot H_2O$ (**6**·H_2O), and $[\{Cu_2(tpyprz)\}Mo_6O_{18}(O_3\text{-}AsC_6H_5)_2]\cdot 2H_2O$ (**7**·$2H_2O$), and the molecular clusters $[\{Cu(2,2'bpy)_2\}_2Mo_{12}O_{34}(O_3AsC_6H_5)_4]\cdot 2.35H_2O$ (**8**·$2.35H_2O$) and $[Cu(o\text{-phen})(H_2O)_3][Cu(o\text{-phen})_2\text{-}Mo_{12}O_{34}(O_3AsC_6H_5)_4]\cdot 3H_2O$ (**9**·$3H_2O$).

Experimental Section

General Considerations. All chemicals were used as obtained without further purification: copper(II) acetate monohydrate, copper(II) sulfate pentahydrate, 2,2′-bipyridine, 1,10-phenanthroline, 2,2′:6′,2″-terpyridine, tetra-2-pyridinylpyrazine, arsenic(V) oxide hydrate, phenylarsonic acid, and *p*-arsanilic acid were purchased from Aldrich; acetic acid, hydrofluoric acid (41−51% HF), and sulfuric acid were purchased from Acros; molybdenum(VI) oxide 99.5% was purchased from Alfa Aesar. All syntheses were carried out in 23 mL poly(tetrafluoroethylene) lined stainless steel containers under autogenous pressure. The reactants were stirred briefly, and initial pH was measured before heating. Water was distilled above 3.0 MΩ in-house using a Barnstead model 525 biopure distilled water center. The reactions' initial and final pHs were measured using Hydrion pH sticks.

Synthesis of $[\{Cu(o\text{-phen})(H_2O)_2\}_2Mo_6O_{18}(O_3AsOH)_2]$ (1). A mixture of MoO_3 (0.098 g, 0.681 mmol), $Cu(CH_3CO_2)_2\cdot H_2O$ (0.044 g, 0.220 mmol), o-phen (0.044 g, 0.222 mmol), $As_2O_5\cdot xH_2O$ (0.052 g, 0.257 mmol), H_2O (10.01 g, 556 mmol), and HF (0.199 g) in the mole ratio 3.10:1.00:1.01:1.17:2527 was stirred briefly before heating to 150 °C for 73 h. The initial and final pH values were 1.5 and 1.0, respectively. Pale blue crystals of **1** were isolated in 50% yield and were suitable for X-ray diffraction. IR (KBr pellet, cm^{-1}): 3510(m, br), 3094(w), 1585(w), 1518(m), 1427(s), 1345-

Scheme 4

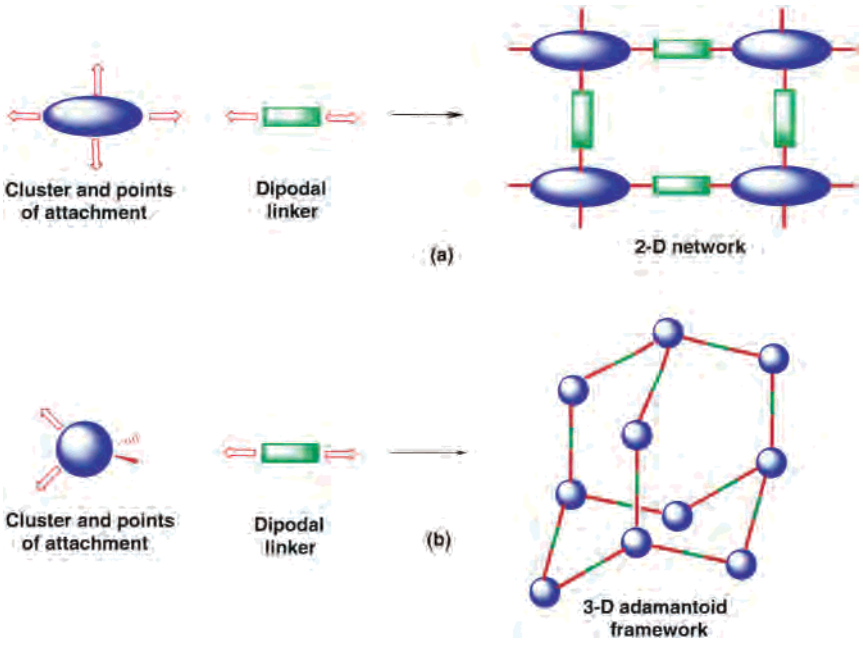

(m), 1146(m), 1109(m), 956(s), 930(vs), 909(m), 877(m), 850(s), 714(s), 585(s).

Synthesis of [{Cu(terpy)}$_2$Mo$_4$O$_{13}$H(O$_3$AsOH)$_2$]·2H$_2$O (2·2H$_2$O). A mixture of MoO_3 (0.161 g, 1.119 mmol), $Cu(CH_3CO_2)_2$·H_2O (0.089 g, 0.446 mmol), terpy (0.104 g, 0.446 mmol), $H_2AsO_3C_6H_4NH_2$ (0.121 g, 0.557 mmol), H_2O (10.08 g, 559 mmol), and concentrated H_2SO_4 (0.261 g) in the mole ratio 2.51:1.00:1.00:1.25:1253 was stirred briefly before heating to 150 °C for 48 h. The initial and final pH were 1.5 and 1.5, respectively. Blue crystals of **2**·2H_2O, suitable for X-ray diffraction, were isolated in 55% yield. IR (KBr pellet, cm^{-1}): 3440(m, br) 3068(m), 1603(m), 1577(m), 1474(m), 1448(m), 1250(w), 1184(w), 1051(m), 1022(w), 930(vs), 915(vs), 878(vs), 815(s), 795(s), 774(m), 711(m), 670(s), 574(m), 488(w).

Synthesis of [{Cu$_2$(tpyprz)(H$_2$O)$_2$}Mo$_6$O$_{18}$(O$_3$AsOH)$_2$]·2H$_2$O (3·2H$_2$O). A solution of MoO_3 (0.191 g, 1.327 mmol), $Cu(CH_3CO_2)_2$·H_2O (0.102 g, 0.511 mmol), tpyprz (0.104 g, 0.268 mmol), As_2O_5·xH_2O (0.157 g, 0.683 mmol), and H_2O (10.01 g, 556 mmol) in the mole ratio 4.95:1.91:1.00:2.55:2075 was stirred briefly before heating to 150 °C for 48 h. The initial and final pH values were 2.0, and 1.5, respectively. Yellow-green crystals of **3**·2H_2O, which were suitable for X-ray diffraction, were isolated in 25% yield. IR (KBr pellet, cm^{-1}): 3446(s), 1559(m), 1418(m), 1202(w), 1031(w), 952(m), 909(s), 813(s), 670(s), and 578(w).

Synthesis of [{Cu(2,2′-bipy)(H$_2$O)}$_2$Mo$_6$O$_{18}$(O$_3$AsC$_6$H$_5$)$_2$]·2H$_2$O (4·2H$_2$O). The reaction of MoO_3 (0.191 g, 1.327 mmol), $Cu(CH_3CO_2)_2$·H_2O (0.044 g, 0.220 mmol), 2,2′-bipy (0.069 g, 0.442 mmol), $H_2O_3AsC_6H_5$ (0.112 g, 0.554 mmol), H_2O (10.01 g, 555 mmol), and HF (0.233 g) in the mole ratio 6.03:1.00:2.01:2.25:2522 at 150 °C for 49.5 h yielded blue crystals of **4**·2H_2O, suitable for X-ray diffraction, in 35% yield. The initial pH was 1.5, and the final pH, 1.0.

Synthesis of [{Cu(o-phen)(H$_2$O)}$_2$Mo$_6$O$_{18}$(O$_3$AsC$_6$H$_5$)$_2$]·4H$_2$O (5·4H$_2$O). A solution of MoO_3 (0.190 g, 1.320 mmol), $Cu(CH_3CO_2)_2$·H_2O (0.092 g, 0.220 mmol), o-phen (0.044 g, 0.222 mmol), $H_2O_3AsC_6H_5$ (0.113 g, 0.559 mmol), H_2O (10.06 g, 558 mmol), and HF (0.234 g) in the mole ratio 5.95:2.08:1.00:2.52:2514 was stirred briefly before heating to 150 °C for 49.5 h. The initial and final pH were 1.5 and 1.0, respectively. Blue crystals of **5**·4H_2O were isolated in 70% yield and were suitable for X-ray diffraction. IR (KBr pellet, cm^{-1}): 3447(s), 1654(m), 1522(m), 915(s), 807(s), 720(m), and 657(s).

Synthesis of [{Cu(terpy)}$_2$Mo$_6$O$_{18}$(O$_3$AsC$_6$H$_5$)$_2$]·H$_2$O (6·H$_2$O). The reaction of MoO_3 (0.186 g, 1.292 mmol), $Cu(CH_3CO_2)_2$·H_2O (0.104 g, 0.521 mmol), terpy (0.120 g, 0.514 mmol), $H_2O_3AsC_6H_5$ (0.264 g, 1.307 mmol), H_2O (10.01 g, 555 mmol), and concentrated H_2SO_4 (0.224 g) in the mole ratio 2.51:1.01:1.00:2.54:1080 at 150 °C for 48 h gave blue crystals of **6**·H_2O suitable for X-ray diffraction in 60% yield. The initial pH was 1.0, and the final pH, 0.5.

Synthesis of [{Cu(tpyprz)}$_2$Mo$_6$O$_{18}$(O$_3$AsC$_6$H$_5$)$_2$]·2H$_2$O (7·2H$_2$O). A mixture of MoO_3 (0.185 g, 1.285 mmol), $Cu(CH_3CO_2)_2$·H_2O (0.101 g, 0.506 mmol), tpyprz (0.100 g, 0.257 mmol), $H_2O_3AsC_6H_5$ (0.264 g, 1.307 mmol), H_2O (10.02 g, 556 mmol), and concentrated H_2SO_4 (0.202 g) in mole ratio 5.00:1.97:1.00:5.09:5163 was stirred briefly before heating to 150 °C for 48 h. The initial and final pHs were 1.5 and 1.0, respectively. Green crystals of **7**·2H_2O, suitable for X-ray diffraction, were isolated in 95% yield. IR (KBr pellet, cm^{-1}): 2568(m, br), 1599(m), 1475(m), 1423(m), 1261(w), 1215(m), 1092(w), 1022(w), 953(s), 916(vs), 901(s), 874(s), 803(vs), 661(vs), 578(m), 521(m).

Synthesis of [{Cu(2,2′-bipy)$_2$}$_2$Mo$_{12}$O$_{34}$(O$_3$AsC$_6$H$_5$)$_4$]·2.35H$_2$O (8·2.35H$_2$O). A reaction of MoO_3 (0.160 g, 1.112 mmol), $Cu(CH_3CO_2)_2$·H_2O (0.045 g, 0.225 mmol), 2,2′-bipy (0.070 g, 0.448 mmol), $H_2O_3AsC_6H_5$ (0.112 g, 0.554 mmol), H_2O (10.01 g, 555 mmol), and CH_3CO_2H (0.197 g) in the mole ratio 4.94:1.00:1.99:2.46:2467 at 150 °C for 48 h yielded blue crystals of **8**·2.35H_2O in 60% yield (initial pH, 2.5; final pH, 2.0).

Synthesis of [Cu(o-phen)(H$_2$O)$_3$][{Cu(o-phen)$_2$}Mo$_{12}$O$_{34}$(O$_3$AsC$_6$H$_5$)$_4$]·3H$_2$O (9·3H$_2$O). A solution of MoO_3 (0.191 g, 1.327 mmol), $Cu(CH_3CO_2)_2$·H_2O (0.089 g, 0.446 mmol), o-phen (0.045 g, 0.227 mmol), $H_2O_3AsC_6H_5$ (0.112 g, 0.554 mmol), H_2O (10.00 g, 555 mmol), and concentrated H_2SO_4 (0.213 g) in the mole ratio 5.85:1.96:1.00:2.44:2444 was stirred briefly before heating to 150 °C for 49.5 h (initial pH, 1.5; final pH, 1.0). Green crystals of **9**·3H_2O, suitable for X-ray diffraction, were isolated in 30% yield. IR (KBr pellet, cm^{-1}): 3447(m), 1560(w), 1429(w), 1089(w), 949(s), 923(s), 869(s), 840(s), 720(w), 590(s), and 490(m).

X-ray Crystallography. Structural measurements for **1**−**9** were performed on a Bruker-AXS SMART-CCD diffractometer at low temperature (87−97 K) using graphite-monochromated Mo Kα radiation (λ(Mo Kα) = 0.71073 Å).[27] The data were corrected for Lorentz and polarization effects and absorption using SADABS.[28] The structures were solved by direct methods. In all cases, all non-hydrogen atoms were refined anisotropically. After all of the non-hydrogen atoms were located, the models were refined against F^2, initially using isotropic and later anisotropic thermal displacement parameters. Hydrogen atoms were introduced in calculated positions and refined isotropically. Neutral atom scattering coefficients and anomalous dispersion corrections were taken from the International Tables, Vol. C. All calculations were performed using SHELXTL crystallographic software packages.[29]

Crystallographic details for the structures of **1**−**9** are summarized in Table 1. Space group assignments and structure solutions and refinements were unexceptional except for the structure of **2**·2H_2O. Absences and reflection symmetry were consistent with the centric *C*2/*m* and the acentric *C*2 space groups. As no satisfactory refinement could be obtained in *C*2/*m*, the acentric choice was pursued. The absence of significant correlations in the matrix of the least squares refinement and a consistent Flack parameter support the choice of space group.

Atomic positional parameters, full tables of bond lengths and angles, and anisotropic temperature factors are available in the Supporting Information. Since the metrical parameters for **1**−**9** are unexceptional, bond length and angle data have not been included in the published manuscript.

Magnetism. Magnetic data were recorded on 17−25 mg samples of compound in the 2−300 K temperature range using a Quantum Design MPMS-5S SQUID spectrometer. Calibrating and operating procedures have been reported previously.[30] The temperature-dependent data were obtained at a magnetic field of H = 1000 Oe.

Thermal Gravimetric Analyses. Thermogravimetric studies were performed using 10−20 mg samples in a Sefaram Tag 24 516 instrument under a 50 mL/min flow of synthetic air. The

(25) Hedman, B. *Acta Crystallogr.* **1980**, *B36*, 2241.
(26) Kwak, W.; Rajkovic, L. M.; Stalick, J. K.; Pope, M. T.; Quicksall, C. O. *Inorg. Chem.* **1976**, *15*, 2778.
(27) *SMART Software Reference Manual*; Siemens Analytical X-ray Instruments, Inc.: Madison, WI, 1994.
(28) Sheldrick, G. M. *SADABS: Program for Empirical Absorption Corrections*; University of Göttingen: Göttingen, Germany, 1996.
(29) Sheldrick, G. M. *SHELXTL96: Program for Refinement of Crystal Structures*; University of Göttingen: Göttingen, Germany, 1996.
(30) O'Connor, C. J. *Prog. Inorg. Chem.* **1979**, *29*, 203.

Table 1. Summary of Crystallographic Data for the Structures of [{Cu(o-phen)(H_2O)$_2$}$_2$$Mo_6O_{18}$($O_3AsOH$)] (**1**), [{Cu(terpy)}$_2$$Mo_4O_{13}$H($AsO_4$)$_2$]·2$H_2O$ (**2**·2H_2O), [{Cu_2(tpyprz)(H_2O)$_2$}Mo_6O_{18}(O_3AsOH)$_2$]·2H_2O (**3**·2H_2O), [{Cu(2,2′-bipy)(H_2O)}$_2$$Mo_6O_{18}$($O_3AsC_6H_5$)$_2$]·2$H_2O$ (**4**·2H_2O), [{Cu(o-phen)(H_2O)}$_2$$Mo_6O_{18}$($O_3AsC_6H_5$)$_2$]·4$H_2O$ (**5**·4H_2O), [{Cu(terpy)}$_2$$Mo_6O_{18}$($O_3AsC_6H_5$)$_2$]·$H_2O$ (**6**·H_2O), [{Cu_2(tpyprz)}Mo_6O_{18}($O_3AsC_6H_5$)$_2$]·2H_2O (**7**·2H_2O), [{Cu(2,2′-bipy)$_2$}$_2$$Mo_{12}O_{34}$($O_3AsC_6H_5$)$_4$]·2.35$H_2O$ (**8**·2.35H_2O), and [Cu(o-phen)(H_2O)$_3$][{Cu(o-phen)$_2$}$Mo_{12}O_{34}$($O_3AsC_6H_5$)$_4$]·3H_2O (**9**·3H_2O)

	1	**2**·2H_2O	**3**·2H_2O	**4**·2H_2O	**5**·4H_2O	**6**·H_2O	**7**·2H_2O	**8**·2.35H_2O	**9**·3H_2O
empirical formula	$C_{12}H_{13}N_2CuMo_3O_{15}As$	$C_{15}H_{13.5}N_3CuMo_2O_{11.5}As_{0.5}$	$C_{12}H_{13}N_3CuMo_3O_{15}As$	$C_{16}H_{17}N_2CuMo_3O_{14}As$	$C_{36}H_{38}N_4Cu_2Mo_6O_{30}As_2$	$C_{21}H_{17}N_3CuMo_3O_{12.5}As$	$C_{18}H_{15}N_3CuMo_3O_{13}As$	$C_{64}H_{56.7}N_8Cu_2Mo_{12}O_{48.35}As_4$	$C_{60}H_{56}N_6Cu_2Mo_{12}O_{52}As_4$
fw	851.52	680.67	865.53	887.6	1859.26	946.66	907.61	3289.84	3271.15
cryst syst	triclinic	monoclinic	triclinic	triclinic	triclinic	monoclinic	monoclinic	tetragonal	monoclinic
space group	$P\bar{1}$	$C2$	$P\bar{1}$	$P\bar{1}$	$P\bar{1}$	$P2_1/n$	$P2_1/n$	$P\bar{4}2_1c$	$P2_1/c$
a, Å	8.5514(4)	23.494(1)	10.144(1)	10.4723(4)	10.2075(5)	13.705(2)	11.1958(5)	28.4822(6)	25.1042(1)
b, Å	9.9091(4)	7.425(4)	10.310(1)	11.2699(4)	14.0640(7)	11.916(1)	15.9472(8)	28.4822(6)	14.5062(6)
c, Å	12.7475(6)	12.692(6)	11.102(1)	11.4438(4)	18.778(1)	17.182(2)	14.0254(7)	22.2344(7)	25.6621(1)
α, deg	86.250(1)	90	103.573(2)	103.696(1)	94.624(1)	90	90	90	90
β, deg	83.849(1)	121.568(1)	107.515(2)	94.708(1)	101.359(1)	99.648(3)	100.854(1)	90	109.681(1)
γ, deg	68.283(1)	90	99.225(2)	114.901(1)	105.369(1)	90	90	90	90
V, Å^3	997.35(8)	1886.3(2)	1042.4(2)	1164.63(7)	2523.1(2)	2766.3(6)	2459.3(2)	18037.3(8)	8799.3(7)
Z	2	4	2	2	2	4	4	8	4
D_{calcd}, g cm^{-3}	2.836	2.397	2.758	2.531	2.447	2.273	2.451	2.423	2.469
μ, mm^{-1}	4.627	3.359	4.431	3.965	3.669	3.345	3.757	3.625	3.717
T, K	92	87(2)	90	91(2)	92(2)	86(2)	90(2)	96(2)	88(2)
λ, Å	0.71073	0.71073	0.71073	0.71073	0.71073	0.71073	0.71073	0.71073	0.71073
R1[a]	0.0400	0.0585	0.0343	0.0329	0.0700	0.0976	0.0447	0.0726	0.1209
wR2[b]	0.0934	0.1138	0.0846	0.0626	0.1226	0.1171	0.0761	0.106	0.1397
Flack		0.04(2)							

[a] $R1 = \sum||F_o| - |F_c||/\sum|F_o|$. [b] $wR2 = \{\sum[w(F_o^2 - F_c^2)^2]/\sum[w(F_o^2)^2]\}^{1/2}$.

temperature was ramped from 20 to 600 °C at a rate of 5 °C/min for the decomposition processes and 1 °C/min for the dehydrations.

Results and Discussion

Synthesis and Spectroscopy. The compounds of this study were prepared by conventional hydrothermal methods, which have been demonstrated to be particularly effective in the preparation of organic−inorganic hybrid materials.[31−34] Under these conditions of temperature and pressure, the differential solubilities in aqueous media of the organic and inorganic starting materials are not problematic, while the structural integrity of the organic components is maintained. The compounds were prepared from mixtures of the appropriate Cu(II) salt, an organoimine ligand, molybdenum trioxide, arsonic acid or an organoarsonate, and water at 150 °C for 48−73 h. The profound structural consequences of addition of a mineralizer, such as acetic acid or H_2SO_4, are manifested in the isolation of the molecular species [{Cu(2,2′-bpy)$_2$}$_2$$Mo_{12}O_{34}$($O_3AsC_6H_5$)$_4$] (**8**) and [{Cu(o-phen)(H_2O)$_3$}{Cu(o-phen)$_2$}$Mo_{12}O_{34}$($O_3AsC_6H_5$)$_4$] (**9**) in the presence of mineralizers and the one-dimensional materials [{Cu(2,2′-bpy)(H_2O)}$_2$$Mo_6O_{18}$($O_3AsC_6H_5$)$_2$] (**4**) and [{Cu(o-phen)(H_2O)}$_2$$Mo_6O_{18}$($O_3AsC_6H_5$)$_2$] (**5**) in the absence of such acids.

The infrared spectra of the compounds exhibit two strong bands in the 800−925 cm^{-1} range associated with ν_{sym}(Mo═O) and ν_{asym}(Mo═O) and a medium to strong intensity band in the 590−690 cm^{-1} region attributed to ν(Mo−O−Mo). A series of medium intensity bands in the 1200−1600 cm^{-1} range is associated with the organoimine ligands.

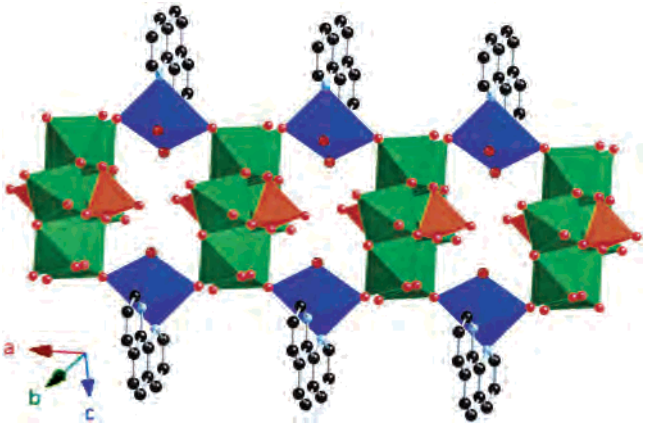

Figure 1. Polyhedral representation of the structure of [{Cu(o-phen)(H_2O)$_2$}$_2$$Mo_6O_{18}$($O_3AsOH$)$_2$] (**1**): copper, blue polyhedra; molybdenum, green octahedra; arsenic, yellow tetrahedra; oxygen, red spheres; nitrogen, light blue spheres; carbon, black spheres. This color scheme is used throughout.

X-ray Structural Studies. The structure of [{Cu(o-phen)(H_2O)$_2$}$_2$$Mo_6O_{18}$($O_3AsOH$)$_2$] (**1**), shown in Figure 1, is representative of the one-dimensional architectures constructed from linked cluster building blocks of this study. The chain consists of {Mo_6O_{18}(O_3AsOH)$_2$}$^{4-}$ clusters bridged by {Cu(o-phen)(H_2O)$_2$}$^{2+}$ subunits. The structure of the molybdoarsonate component is essentially identical to that previously reported for the salts of {Mo_6O_{18}(AsO_4)$_2$}$^{6-}$.[35−38] The cluster consists of a ring of *cis*-edge sharing {MoO_6} octahedra, capped on both faces by {O_3AsOH} tetrahedra. Each arsonate subunit shares three oxo-groups with the molybdate ring. In turn, each of these oxo-groups adopts the

(31) Laudise, R. A. *Chem. Eng. News* **1987**, *65*, 30.
(32) Lobachev, A. N. *Crystallization Processes Under Hydrothermal Conditions*; Consultants Bureau: New York, 1973.
(33) Gopalakrishnan, J. *Chem. Mater.* **1995**, *7*, 1265.
(34) Hagrman, D.; Hagrman, P.; Zubieta, J. *Comments Inorg. Chem.* **1999**, *21*, 225.
(35) Hedman, B. *Acta Crystallogr.* **1980**, *B36*, 2241.
(36) Nishikawa, K.; Sasaki, Y. *Chem. Lett.* **1975**, 1185.
(37) Pope, M. T.; Quicksall, C. O.; Kwak, W.; Rajkovic, L. M.; Stalick, J. K.; Barkigia, K. M.; Scully, T. F. *J. Less-Common Met.* **1977**, *54*, 129.
(38) Barkigia, K. M.; Rajkovic-Blazer, L. M.; Pope, M. T.; Quicksal, C. O. *Inorg. Chem.* **1980**, *19*, 2531.

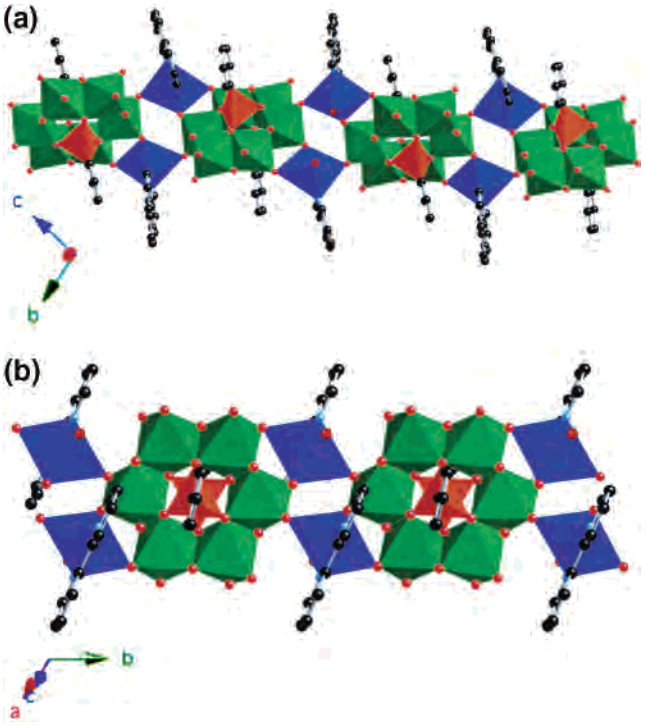

Figure 2. (a) One-dimensional structure of $[\{Cu(o\text{-phen})(H_2O)\}_2Mo_6O_{18}(O_3AsC_6H_5)_2]\cdot 4H_2O$ (**5**·H_2O). (b) View of the structure of $[\{Cu(2,2'\text{-bpy})(H_2O)\}_2Mo_6O_{18}(O_3AsC_6H_5)_2]\cdot 2H_2O$ (**4**·$2H_2O$).

μ^3 bridging mode, linking two molybdenum sites and the arsenic. The fourth oxygen of the tetrahedral arsenic unit is pendant and protonated, as indicated by the As−O distance of 1.71 Å and by charge-balance considerations.

The copper(II) sites adopt the common "4 + 2" axially distorted geometry, characteristic of this d^9 Jahn−Teller cation. The $\{CuO_4N_2\}$ site is defined by two oxo-groups from adjacent $\{Mo_6O_{18}(O_3AsOH)_2\}^{4-}$ clusters, two nitrogen donors from the chelating phenanthroline ligand, and two oxygen donors from aqua ligands. Each molybdoarsonate cluster employs four terminal oxo-groups on four distinct Mo(VI) sites to link to the Cu(II) sites.

The copper polyhedra are disposed above and below the $\{Mo_6O_{24}\}$ central ring, with the organic ligands radiating outward from the chain propagation vector. As a result of this connectivity pattern, the {As−OH} unit is tucked into the Cu(II)−aqua domain of the chain, exhibiting hydrogen-bonding to the terminal oxo-group of a molybdenum site on an adjacent cluster unit (O6···O2, 2.74 Å). The aqua ligands also exhibit hydrogen-bonding interactions with the cluster units. One water group displays short contacts to an oxo-group bridging two Mo sites of one neighboring cluster and to an oxygen bridging As and Mo sites on the second adjacent cluster (O14···O1 and O14···O8, 2.62 and 2.76 Å, respectively). The second aqua ligand engages in hydrogen-bonding to a terminal oxo-group of an adjacent chain (O15···O10, 2.76 Å).

Similar chain structures to that of **1** are observed for $[\{Cu(2,2'\text{-bpy})(H_2O)\}_2Mo_6O_{18}(O_3AsC_6H_5)_2]\cdot 2H_2O$ (**4**·$2H_2O$) and $[\{Cu(o\text{-phen})(H_2O)\}_2Mo_6O_{18}(O_3AsC_6H_5)_2]\cdot 4H_2O$ (**5**·$4H_2O$). As shown in Figure 2a for **5**, the structures of **4** and **5** are constructed of $\{Mo_6O_{18}(O_3AsC_6H_5)_2\}^{4-}$ clusters linked through

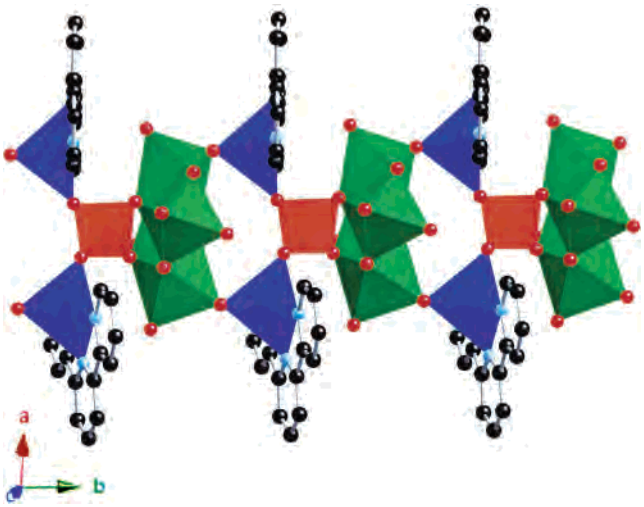

Figure 3. Structure of $[\{Cu(terpy)\}_2Mo_4O_{13}H(AsO_4)]\cdot 2H_2O$ (**2**·$2H_2O$).

$\{Cu(2,2'\text{-bpy})(H_2O)\}^{2+}$ and $\{Cu(o\text{-phen})(H_2O)\}^{2+}$ subunits. The molybdoarsonate clusters of **4** and **5** are identical to that of **1** with the exception of the phenyl substituent of **4** and **5** replacing the pendant OH group of **1**. However, the mode of attachment of the Cu(II)−ligand subunits for **4** and **5**, as well as the relative orientations of the clusters and bridging subunits, are quite distinct from those of **1**. The distorted "4 + 2" $\{CuO_4N_2\}$ polyhedra of **4** and **5** exhibit linkages to three cluster oxo-groups, rather than two as seen for **1**, and coordinate one aqua ligand, rather than two observed in the structure of **1**. Consequently, each $\{Mo_6O_{24}\}$ ring shares six oxo-groups with the bridging Cu(II)−ligand subunits.

The steric constraints introduced by substituting the bulky C_6H_5 substituent for OH on the As center are also apparent in the overall chain structure. The $\{As-C_6H_5\}$ moiety can no longer tuck into the Cu(II)−ligand domain. Consequently, the $\{As-C_6H_5\}$ vector and the Cu−ligand vectors are now approximately parallel and radiate outward from the $\{Cu_2Mo_6O_{24}\}$ chain. However, it is curious that the chain geometries of **4** and **5** are not identical, as illustrated in Figure 2a,b. Thus, in the case of **4**, the $\{Mo_6O_{24}\}$ ring planes are aligned in parallel, while in **5** alternate rings along the chain are rotated by approximately 90°.

The fourth one-dimensional structure, $[\{Cu(terpy)\}_2Mo_4O_{13}H(AsO_4)]\cdot 2H_2O$ (**2**·$2H_2O$), illustrates the profound structural consequences of ligand identity and reaction conditions. As shown in Figure 3, the common $\{Mo_6O_{18}(O_3AsR)_2\}^{4-}$ building block is not observed for **2**. Rather, the chain is constructed from $\{HMo_4O_{13}(AsO_4)\}^{4-}$ clusters linked through $\{Cu(terpy)\}^{2+}$ subunits into a one-dimensional chain.

The molybdate subunit consists of an unusual tetranuclear $\{HMo_4O_{15}\}$ cluster,[39] shown in Figure 4. The cluster is a compact assembly of edge- and face-sharing octahedra. Each octahedron shares a face with an adjacent $\{MoO_6\}$ unit, an edge with a second, and a single oxo-group with the third. The central oxo-group of the cluster adopts a μ^4-bridging mode. The $\{HMo_4O_{15}\}$ cluster of **2** is essentially identical to that of tetramolybdodimethylarsinate derivative $[HMo_4O_{15}$-

(39) Hsu, K.-F.; Wang, S.-L. *Inorg. Chem.* **1997**, *36*, 3049.

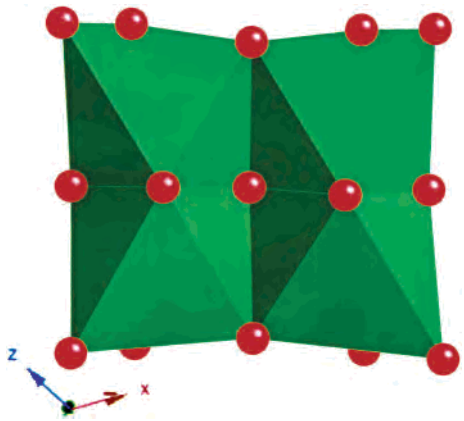

Figure 4. $\{HMo_4O_{15}\}$ cluster of **2**.

As-$Me_2]^{2-}$.[38] In this previous study, the protonation site was established by neutron diffraction as the basal μ_4-oxo group. Valence sum calculations[40] on **2** also suggest that the μ_4-oxo group O6 is the protonating site, as the valence for O6 is ca. 0.8, while those of all remaining oxygen atoms fall in the range 1.7−2.0.

Each molybdate subunit contributes two oxo-groups to the As tetrahedron and two oxo-groups to the bridging $\{Cu(terpy)\}^{2+}$ subunit; consequently, each molybdate subunit exhibits four points of attachment. In contrast to the $\{O_3AsOH\}^{2-}$ subunit of **1**, the $\{AsO_4\}$ tetrahedron of **2** employs all four oxo-groups in bridging to metal sites. In addition to the two oxo-groups linking to the molybdate subunit, the remaining two oxygen atoms bridge to two copper sites.

The copper(II) sites adopt $\{CuN_3O_2\}$ "4 + 1" distorted square pyramidal geometry, with the basal plane defined by the three nitrogen donors of the terpy ligand and one oxo-group and the second oxo-group in the apical position. In contrast to structures **1**, **4**, and **5**, the Cu(II) sites of **2** do not bridge Mo centers of adjacent clusters, but rather link to an As site of one $\{HMo_4O_{13}(AsO_4)\}^{4-}$ subunit and a molybdenum center of a second.

The structures of compounds **1**, **4**, and **5** reveal that the $\{Mo_6O_{18}(O_3AsR)_2\}^{4-}$ cluster may exhibit four to six points of attachment about the $\{Mo_6O_{24}\}$ girdle. As anticipated, the larger cluster volume is associated with an expanded number of attachment sites when compared to the phosphorus based series $\{Mo_5O_{15}(O_3PR)_2\}^{4-}$ which generally exhibit two attachment points and a maximum of four. This observation led to the expectation that the arsenate-based cluster unit could serve as a building block for expansion into two-dimensional structures when combined with an appropriate binucleating ligand for the Cu−ligand component. This expectation has been realized in the structures of $[\{Cu_2(tpyprz)(H_2O)_2\}Mo_6O_{18}(O_3AsOH)_2]\cdot 2H_2O$ (**3**·$2H_2O$) and $[\{Cu_2(tpyprz)\}Mo_6O_{18}(O_3AsC_6H_5)_2]\cdot 2H_2O$ (**7**·$2H_2O$).

As shown in Figure 5, the structure of **3** is constructed from $\{Mo_6O_{18}(O_3AsOH)_2\}^{4-}$ clusters linked through $\{Cu_2(tpyprz)(H_2O)_2\}^{4+}$ units into a two-dimensional architecture. Each molybdoarsonate cluster exhibits four points of attachment to Cu(II) sites, using four molybdenum centers of the ring. In turn, each Cu(II) site bridges two adjacent clusters; consequently, every binuclear $\{Cu_2(tpyprz)(H_2O)_2\}^{4+}$ subunit is associated with four clusters. The Cu(II) sites exhibit "4 + 2" $\{CuO_3N_3\}$ geometry, defined by two oxo-groups bridging to Mo sites, three nitrogen donors of one terminus of the tetra-2-pyridinylpyrazine ligand, and an aqua ligand.

The linkage of clusters and Cu subunits produces a coplanar disposition of the $\{Mo_6O_{24}\}$ rings and the copper−aqua subunits. The coordinated water molecules are thus tucked into intralamellar cavities with hydrogen bonding in hydrogen-bonding to terminal oxo-groups within the layer (O99···O12 and O99···O12a, 2.83 and 2.84 Å, respectively). The {As−OH} groups and the pyridyl rings of the tpyprz ligands project above and below the Cu/Mo/O layers.

The structure of compound **7** is grossly similar to that of **3**, as shown in Figure 6. Again, the two-dimensional connectivity is provided by the prototypical $\{Mo_6O_{18}(O_3AsR)_2\}^{4-}$ clusters linked through $\{Cu_2(tpyprz)\}^{4+}$ units. However, each cluster now enjoys six loci of attachment to

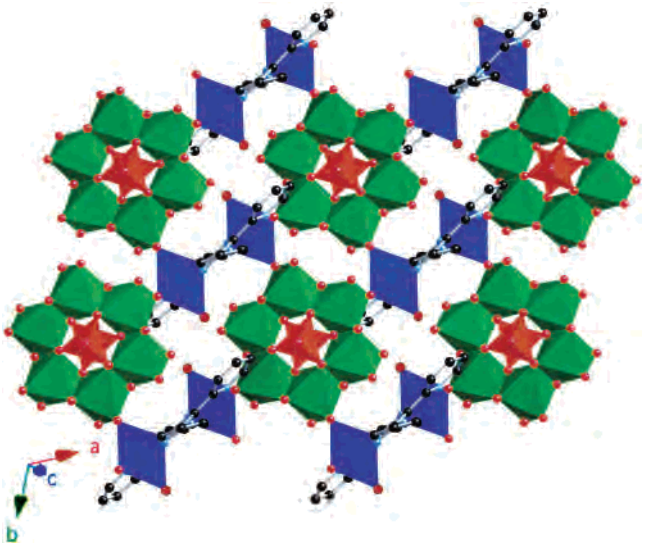

Figure 5. Polyhedral representation of the structure of $[\{Cu_2(tpyprz)(H_2O)_2\}Mo_6O_{18}(O_3AsOH)_2)\cdot 2H_2O$ (**3**·$2H_2O$).

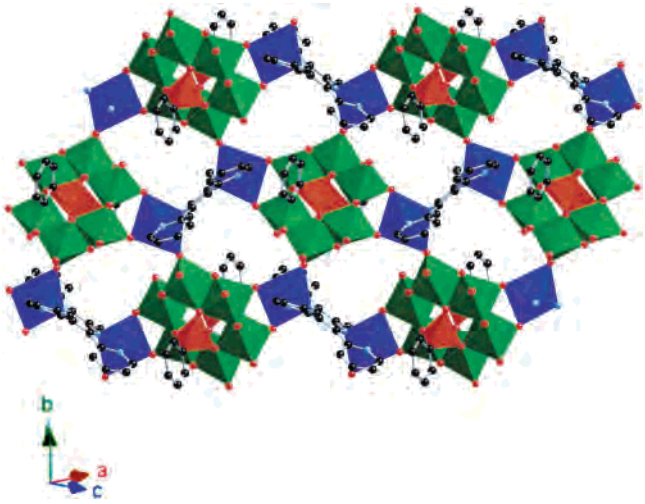

Figure 6. Two-dimensional structure of $[\{Cu_2(tpyprz)\}Mo_6O_{18}(O_3AsC_6H_5)_2]\cdot 2H_2O$ (**7**·$2H_2O$).

(40) Brown, I. D.; Alternatt, D. *Acta Crystallogr.* **1985**, *B41*, 244.

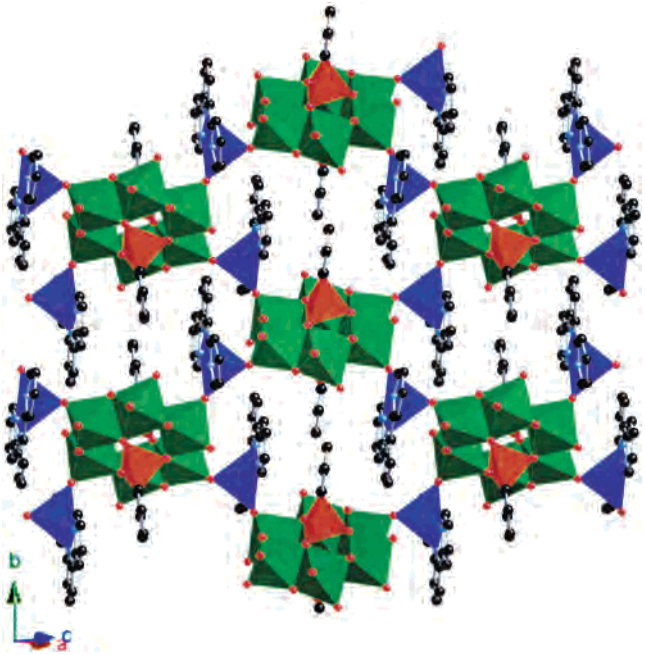

Figure 7. Polyhedral representation of the structure of $[\{Cu(terpy)\}_2Mo_6O_{18}(O_3AsC_6H_5)_2]\cdot H_2O$ (**6**·H_2O).

the Cu sites, rather than four as in compound **3**. Each copper site participates in corner sharing with two Mo sites of one cluster and one of an adjacent cluster. Each cluster is associated with four binuclear copper units, and each binuclear copper−ligand site, with four clusters.

As in **3**, the Cu(II) geometry is the "4 + 2" $\{CuO_3N_3\}$ type, defined by three oxo-groups shared with Mo sites and three nitrogen donors of the ligand. Since the Cu coordination in **7** is completed by oxo-groups, no aqua ligation is observed, as was the case for **3**.

The linkage of a Cu polyhedron to two adjacent $\{MoO_6\}$ octahedra of a cluster results in a ruffling of the layer of **7**, in contrast to the planarity of the Cu/Mo/O network of **3**. This feature is most evident in the {As−C(phenyl)} vector of **7**, which makes an angle of ca. 65° with respect to the Cu/Mo/O least squares plane, whereas the {As−OH} vector of **3** is normal to the Cu/Mo/O network of **3**. The structure of **7** is in fact not related to that of **3** by simple dehydration and attachment of the resultant vacant Cu coordination site of the binuclear unit to an oxo-group of the cluster. This is evident in the absence in **7** of the $\{Cu_2Mo_4O_6\}$ ring substructure observed for **3**. The layer of **7** is also more compact than that of **3** since the free volume required to capture the aqua ligand is no longer required.

Somewhat unexpectedly, the structure of $[\{Cu(terpy)\}_2Mo_6O_{18}(O_3AsC_6H_5)_2]\cdot H_2O$ (**6**·H_2O) is also two-dimensional (Figure 7). The structure is constructed from the anticipated $\{Mo_6O_{18}(O_3AsC_6H_5)_2\}^{4-}$ and $\{Cu(terpy)\}^{2+}$ building blocks. However, in contrast to the structure of **1**, **4**, and **5**, the four $\{Cu(terpy)\}^{2+}$ units associated with each molybdoarsonate cluster bridge to four adjacent clusters, rather than two.

The distinct structural characteristics of **1**, **4**, **5**, and **6** are clearly manifested in their bimetallic oxide ring substructures. Thus, **1** exhibits a 16-membered $\{Cu_2Mo_6O_8\}$ cyclic motif, while **4** and **5** are characterized by eight-membered $\{Cu_2Mo_2O_4\}$ rings. In contrast, **6** is characterized by a greatly expanded metal oxide annular substructure $\{Cu_4Mo_{10}O_{14}\}$, that is, a 14 polyhedral connect. The large ring size is related to the need to accommodate the central ring of the terpy ligand in an intralamellar domain.

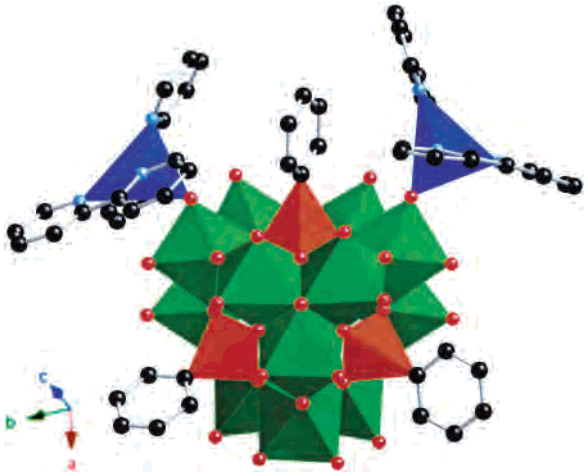

Figure 8. Molecular cluster of $[\{Cu(2,2'\text{-bpy})_2\}_2Mo_{12}O_{34}(O_3AsC_6H_5)_4]\cdot 2.35H_2O$ (**8**·$2.35H_2O$).

Minor variations in reaction conditions were found to result in molecular clusters. $[\{Cu(2,2'\text{-bpy})_2\}_2Mo_{12}O_{34}(O_3AsC_6H_5)_4]\cdot 2.35H_2O$ (**8**·$2.35H_2O$) and $[Cu(o\text{-phen})(H_2O)_3][Cu(o\text{-phen})_2Mo_{12}O_{34}(O_3AsC_6H_5)_4]\cdot 3H_2O$ (**9**·$3H_2O$) are characteristic of such materials.

The structure of **8**, shown in Figure 8, consists of a $[Mo_{12}O_{34}(O_3AsC_6H_5)_4]^{4-}$ cluster, decorated by two $\{Cu(2,2'\text{-bpy})_2\}^{2+}$ units. The structure of the cluster is essentially identical to those of the previously reported $[Mo_{12}O_{34}(O_3AsOH)_4]^{4-}$ [41] and $[Mo_{12}O_{34}(O_3AsC_6H_4NH_3)_4]$.[42] The molybdoarsonate cluster is constructed of four $\{Mo_3O_{12}\}$ subunits of *cis*-edge sharing $\{MoO_6\}$ octahedra. Each trinuclear subunit exhibits one corner-sharing interaction to each of the three adjacent trinuclear motifs, to produce a tetrahedral array of trinuclear units. The $\{Mo_6O_6\}$ rings formed at the junctions of three adjacent trinuclear units result in large triangular cavities which are capped by the $\{AsC_6H_5\}$ groups. In the case of **8**, two Mo sites from two adjacent trinuclear units bridge through terminal oxo-groups to two $\{Cu(bpy)_2\}^{2+}$ fragments. The Cu(II) sites display "4 + 1" distorted square pyramidal geometry, defined by four nitrogen atoms from the two bipyridine chelates and the oxo-group.

The structure of **9**, shown in Figure 9, is similar to that of **8**, with the exception that a single $\{Cu(phen)_2\}^{2+}$ polyhedron attaches itself to the $\{Mo_{12}O_{34}(O_3AsC_6H_5)_4\}^{4-}$ cluster. Charge balance is achieved by incorporating the second Cu(II) site, as a discrete $\{Cu(phen)(H_2O)_3\}^{2+}$ cation.

The structures of **1**−**9** exhibit a considerable range of component substructures and polyhedral connectivities, as summarized in Table 2. While the molecular species **8** and

(41) Nishikawa, K.; Sasaki, Y. *Chem. Lett.* **1975**, 1185.
(42) Pope, M. T.; Quicksall, C. O.; Kwak, W.; Rajković, L. M.; Stalick, J. K.; Barkigia, K. M.; Scully, T. F. *J. Less-Common Metals* **1977**, *54*, 129.

Table 2. Selected Structural Characteristics of the Copper(II)−Organoimine/Molybdoarsonates of This Study

compd	dimensionality	copper geometry	copper−molybdate substructure	molybdoarsonate substructure
$[\{Cu(2,2'\text{-bpy})_2\}_2Mo_{12}O_{34}(O_3AsC_6H_5)_4]\cdot 2.35H_2O$ (**8**·2.34H_2O)	molecular	$\{CuN_4O\}$ "4 + 1" square pyramid	$[\{Cu(2,2'\text{-bpy})_2\}_2Mo_{12}O_{34}]^{8+}$ cluster	$\{Mo_{12}O_{34}(O_3AsC_6H_4)_4\}^{4-}$ cluster
$[\{Cu(o\text{-phen})(H_2O)_3\}\{Cu(o\text{-phen})_2\}Mo_{12}O_{34}(O_3AsC_6H_5)_4]\cdot 3H_2O$ (**9**·3H_2O)	molecular	$\{CuN_4O\}$ "4 + 1" square pyramid	$[\{Cu(o\text{-phen})_2\}Mo_{12}O_{34}]^{6+}$ cluster	$\{Mo_{12}O_{34}(O_3AsC_6H_4)_4\}^{4-}$ cluster
$[\{Cu(o\text{-phen})(H_2O)_2\}_2Mo_6O_{18}(O_3AsOH)_2]$ (**1**)	1-D	$\{CuN_2O_4\}$ "4 +2" octahedron	$[\{Cu(o\text{-phen})\}_2Mo_6O_{18}]_n^{4n+}$ chain	$\{Mo_6O_{18}(O_3AsOH)_2\}^{4-}$ cluster
$[\{Cu(2,2'\text{-bpy})(H_2O)\}_2Mo_6O_{18}(O_3AsC_6H_5)_2]\cdot 2H_2O$ (**4**·2H_2O)	1-D	$\{CuN_2O_4\}$ "4 + 2" octahedron	$[\{Cu(2,2'\text{-bpy})\}_2Mo_6O_{18}]_n^{4n+}$ chains	$\{Mo_6O_{18}(O_3AsC_6H_5)_2^{4-}$ cluster
$[\{Cu(o\text{-phen})(H_2O)\}_2Mo_6O_{18}(O_3AsC_6H_5)_2]\cdot 4H_2O$ (**5**·4H_2O)	1-D	$\{CuN_2O_4\}$ "4 + 2" octahedra	$[\{Cu(o\text{-phen})\}_2Mo_6O_{18}]_n^{4n+}$ chains	$\{Mo_6O_{18}(O_3AsC_6H_5)_2\}^{4-}$ clusters
$[\{Cu(terpy)\}_2Mo_4O_{13}H(AsO_4)]\cdot 2H_2O$ (**2**·2H_2O)	1-D	$\{CuN_3O_2\}$ "4 + 1" square pyramid	$[\{Cu(terpy)\}_2Mo_6O_{13}H]]^{3+}$ cluster	$\{Mo_4O_{13}H(AsO_4)\}^{4-}$ cluster
$[\{Cu_2(tpyprz)(H_2O)_2\}Mo_6O_{18}(O_3AsOH)_2]\cdot 2H_2O$ (**3**·2H_2O)	2-D	$\{CuN_3O_3\}$ "4 + 2" octahedron	$[\{Cu_2(tpytrz)\}Mo_6O_{18}]_n^{4n+}$ network	$\{Mo_6O_{18}(O_3AsOH)_2\}^{4-}$ cluster
$[\{Cu(terpy)\}_2Mo_6O_{18}(O_3AsC_6H_5)_2]\cdot H_2O$ (**6**·H_2O)	2-D	$\{CuN_3O_2\}$ "4 + 1" square pyramid	$[\{Cu(terpy)\}_2Mo_6O_{18}]_n^{4n+}$ network	$\{Mo_6O_{18}(O_3AsC_6H_4)_2^{4-}$ cluster
$[\{Cu_2(tpyprz)\}Mo_6O_{18}(O_3AsC_6H_5)_2]\cdot 2H_2O$ (**7**·2H_2O)	2-D	$\{CuN_3O_3\}$ "4 + 2" octahedron	$[\{Cu_2(tpyprz)\}Mo_6O_{18}]_n^{4n+}$ network	$\{Mo_6O_{18}(O_3AsC_6H_5)_2\}^{4-}$ cluster

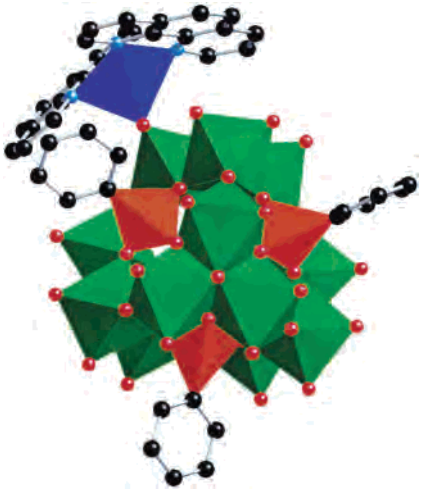

Figure 9. Molecular anion $[\{Cu(o\text{-phen})_2\}Mo_{12}O_{34}(O_3AsC_6H_5)_4]^{2-}$ of **9**·3H_2O.

9 are constructed from the $[Mo_{12}O_{34}(O_3AsR)_4]^{4-}$ core, the two-dimensional materials **3**, **6**, and **7** and the one-dimensional materials (**1**, **4**, and **5**) with the exception of **2** contain as a common structural motif the $\{Mo_6O_{18}(O_3AsR)_2\}^{4-}$ cluster. The imbedding of the unusual $\{Mo_4O_{13}H(AsO_4)_2\}^{4-}$ cluster in the chain structure of **2** illustrates the structural versatility and occasional unpredictability of the structural chemistry.

It is also noteworthy that the copper geometry exhibits considerable variability within this set of compounds. The Jahn−Teller distorted five coordinate sites display $\{CuN_4O\}$ and $\{CuN_3O_2\}$ coordination geometries, while the six coordinate "4 + 2" sites provide $\{CuN_2O_4\}$ and $\{CuN_3O_3\}$ geometries. The copper sites also exhibit variable coordination to aqua ligands, $\{Cu(LL)(H_2O)_x\}^{2+}$ where $x = 0$, 1, 2, or 3.

A recurrent structural motif in the solid state chemistry of the Cu(II)−organoimine/molybdophosphate and Cu(II)−organoimine/molybdoarsonate families is the presence of the $\{(Mo_5O_{15})(O_3PR)_2\}^{4-}$ and $\{(Mo_6O_{18})(O_3AsR)_2\}^{4-}$ clusters, respectively, as building blocks. As shown in Table 3, there are now some 18 examples of materials of this type. These may be classified according to the linkage mode between cluster sites. Thus, clusters linked exclusively through mononuclear $\{Cu(LL)_x(H_2O)_y\}^{2+}$ subunits are classified as type Ia for one-dimensional structures and type Ib for two-dimensional networks. Clusters linked through binuclear $\{Cu_2(tpyprz)(H_2O)_x\}^{4+}$ dipodal tethers are classified as type IIa and IIb for chains and networks, respectively. Finally, clusters linked through both Cu subunits and the organic tethers of the $\{O_3E(CH_2)_nEO_3\}^{4-}$ subunits are identified as type IIIa and IIIb for two-dimensional materials and three-dimensional frameworks, respectively.

Two characteristics of the structures of these families of materials are noteworthy. The number of loci on the surface of the molybdate cluster for attachment to copper sites should reflect the size of the cluster and hence the availability of free oxo-groups on the cluster surface. Consequently, the $\{Mo_6O_{18}(O_3AsR)_2\}^{4-}$ core should in general accommodate more Mo−O−Cu interactions than the pentamolybdate core $\{Mo_5O_{13}(O_3PR)_2\}^{4-}$. In fact, the molybdophosphonate core exhibits considerable variability with respect to the number of Cu attachments with 2, 3, and 4 Mo−O−Cu bonds per cluster observed in the series. In contrast, the molybdoarsonate cluster exhibits 4 or 6 points of attachment, in accord with its larger volume. However, beyond the obvious observation that two Mo−O−Cu linkages/clusters result in a one-dimensional structure, there is no correlation between points of attachment and overall dimensionality. Thus, compound **4** exhibits six Mo−O−Cu bonds/clusters and is

Table 3. Summary of Structural Characteristics of Materials Constructed from $\{Mo_5O_{15}(O_3PR)_2\}^{4-}$ and $\{Mo_6O_{18}(O_3AsR)_2\}^{4-}$ Cluster Building Blocks

compd	class	overall dimensionality	no. attachment points/cluster		no. Cu−O−Mo bonds/Cu	no. clusters bridged/Cu
$[\{Cu(bpy)\}_2\{Cu(bpy)(H_2O)\}Mo_5O_{15}\{O_3P(CH_2)_4PO_3\}]$	type Ia	1-D	2	1	1	0
$[\{Cu(terpy)(H_2O)\}_2Mo_5O_{15}(O_3PCH_2CH_2PO_3)]$	type Ia	1-D	2	0	1	0
$[\{Cu(phen)_2\}\{Cu(phen)(H_2O)\}Mo_5O_{15}\{O_3P(CH_2)_3PO_3\}]$	type Ia	1-D	2	0	1	0
$[\{Cu(phen)(H_2O)_2\}_2Mo_6O_{18}(O_3AsOH)_2]$	type Ia	1-D	4	0	2	2
$[\{Cu(bpy)(H_2O)\}_2Mo_6O_{18}(O_3AsC_6H_5)_2]$	type Ia	1-D	6	0	3	2
$[\{Cu(phen)(H_2O)\}_2Mo_6O_{18}(O_3AsC_6H_5)_2]$	type Ia	1-D	6	0	3	2
$[\{Cu(terpy)\}_2Mo_5O_{15}\{O_3P(CH_2)_3PO_3\}]$	type Ib	2-D	4	0	2	2
$[\{Cu(terpy)\}_2Mo_6O_{18}(O_3AsC_6H_5)_2]$	type Ib	2-D	4	0	2	2
$[\{Cu_2(tpypyz)(H_2O)_3\}Mo_5O_{15}(HOPO_3)(O_3PCH_2CO_2H)]$	type IIa	1-D	2	0	2 and 0	2 and 0
$[\{Cu_2(tpypyz)H_2O)_2\}Mo_6O_{18}(O_3AsOH)_2]$	type IIa	1-D	2	0	1	0
$[\{Cu_2(tpypyz)(H_2O)_2\}Mo_6O_{18}(O_3AsOH)_2]$	type IIb	2-D	4	0	2	2
$[\{Cu_2(tpypyz)\}Mo_6O_{18}(O_3AsC_6H_5)_2]$	type IIb	2-D	6	0	3	2
$[\{Cu_2(tpypyz)(H_2O)_2\}Mo_5O_{15}(HOPO_3)_2]\cdot 2H_2O$	type IIb	2-D	4	0	2	2
$[\{Cu_2(tpypyz)(H_2O)_3\}Mo_5O_{15}(HOPO_3)_2]$	type IIb	2-D	3	0	2 and 1	2 and 0
$[\{Cu(tpypyz)(H_2O)_2\}Mo_5O_{15}(HOPO_3)_2]$	type IIc	3-D	4	0	2	2
$[\{Cu_2(tpypyz)(H_2O)_2\}Mo_5O_{15}(O_3PCH_2CH_2PO_3)]$	type IIIa	2-D	3	1	2 and 1	2 and 0
$[\{Cu_2(tpypyz)(H_2O)_2\}Mo_5O_{15}\{O_3P(CH_2)_3PO_3\}]$	type IIIb	3-D	4	0	2	2
$[\{Cu_2(tpypyz)(H_2O)_2\}Mo_5O_{15}\{O_3P(CH_2)_4PO_3\}]$	type IIIb	3-D	4	0	2	2

one-dimensional, while $[\{(tpyprz)(H_2O)_2\}Mo_5O_{15}(HOPO_3)_2]$ has four attachment points and is three-dimensional. Such characteristics render predictability of intimate structural details somewhat elusive.

Magnetism. The molecular species **8** and **9** exhibit Curie paramagnetism with the susceptibility dependence as temperature given by

$$\chi = C/T + \mathrm{TI} \quad (1)$$

The best fits for compounds **8** and **9** are given by $C = 0.781$ emu K/(Oe mol), $g = 2.10$, (TI = Temperature Independent Paramagnetism) TI $= -0.00021$ cm^3/mol and $C = 0.803$ emu K/(Oe mol), $g = 2.07$, TI $= -0.00011$ cm^3/mol, respectively. The effective moments at 300 K for **8** and **9** are 1.83 and 1.79 μ_B, respectively.

The magnetic behavior of $[\{Cu(o\text{-}phen)(H_2O)\}_2Mo_6O_{18}(O_3AsC_6H_5)_2]\cdot 4H_2O$ (**5**·4H$_2$O) shown in Figure 10a is also consistent with Curie paramagnetism, and the data were fit to the Curie−Weiss law:

$$\chi = C/[(T - \Theta)] + \mathrm{TI} \quad (2)$$

The best fit for **5** gave the values $C = 0.900$ emu K/(Oe mol), $g = 2.19$, TIP $= -0.00115$ emu/(Oe mol), and $\Theta = 0.0$.

In contrast, $[\{Cu_2(tpyprz)(H_2O)_2\}Mo_6O_{18}(O_3AsOH)_2]\cdot 2H_2O$ (**3**·2H$_2$O) exhibits weak antiferromagnetic coupling between Cu(II) sites (Figure 10b). In this case, the fit to the Curie−Weiss law gives $C = 0.459$ emuK/(Oe mol), $g = 2.21$, TIP $= -0.00066$, and $\Theta = -0.9$. The antiferromagnetic coupling presumably occurs through the π system of the tpyprz binucleating ligand, as previously observed for the copper(II)−tpyprz/molybdophosphonate family.[43] However, in the latter materials, the antiferromagnetic interactions are significantly more pronounced giving rise to maxima in the χ versus T plots at 30−35 K and J/k_B values of ca. −25 K.

The compounds **3** and **7** which contain the $\{Cu_2(tpyprz)\}^{4+}$ binuclear subunit in a two-dimensional structure exhibit similar magnetic properties as illustrated in Figure 10c for **7**. The susceptibility shows a maximum at ca. 30 K, consistent with the presence of antiferromagnetic interactions. The best fit to the data is obtained using the Heisenberg dimer model ($S = {}^1/_2$):

$$\chi = (1-x)\frac{N_A g^2 \mu_B{}^2}{k_B T}\frac{2\exp\left(\frac{2J}{k_B T}\right)}{1+3\exp\left(\frac{2J}{k_B T}\right)} + x\frac{N_A g^2 \mu_B{}^2}{2k_B T} + \mathrm{TI} \quad (3)$$

with $g = 2.16$, $J/k_B = -7.3$ K, TI $= -0.00071$ cm^3/mol, and $x = 0.001$.

The range of magnetic behaviors displayed by the compounds of this study is completed by **1**. As shown in Figure 10d, the temperature dependence of the molar susceptibility of **1** exhibits a broad maximum at 8 K, indicative of antiferromagnetic interactions. The data were fit to the Heisenberg linear antiferromagnetic chain model ($S = {}^1/_2$) using eq 4 where $y = J/(k_B T)$.

$$\chi = 2\frac{N_A g^2 \mu_B{}^2}{k_B T}\left\{(1-x)\left[\frac{0.25 + 0.14995y + 0.30094y^2}{1 + 1.9862y + 0.68854y^2 + 6.062y^3}\right] + \frac{x}{4}\right\} + \mathrm{TI} \quad (4)$$

The best fit gave $g = 2.56$, $J/k_B = -6.7$ K, and TI $= 0.0015$ cm^3/mol. The effective moment at 300 K is 3.09 μ_B (2.18 μ_B per Cu atom).

Thermal Behavior. The prototypical thermal decomposition profile for the loss of the organic components and for collapse of the molybdoarsonate substructures of the compounds of this study is provided by $[\{Cu(o\text{-}phen)(H_2O)_2\}_2Mo_6O_{18}(O_3AsOH)_2]$ (**1**). The compound is stable to 340 °C, whereupon there occurs a weight loss of ca. 5% associated with the loss of the copper bound aqua ligands (4.2%, calculated). This dehydration process is followed by a weight loss of ca. 34% between 380 and 430 °C, corresponding to the loss of the organic components and As_2O_3 (32.8%, calculated). The sublimation of As_2O_3 from arsonate contain-

(43) Burkholder, E.; Golub, V.; O'Connor, C. J.; Zubieta, J. **2003**, *42*, 6729.

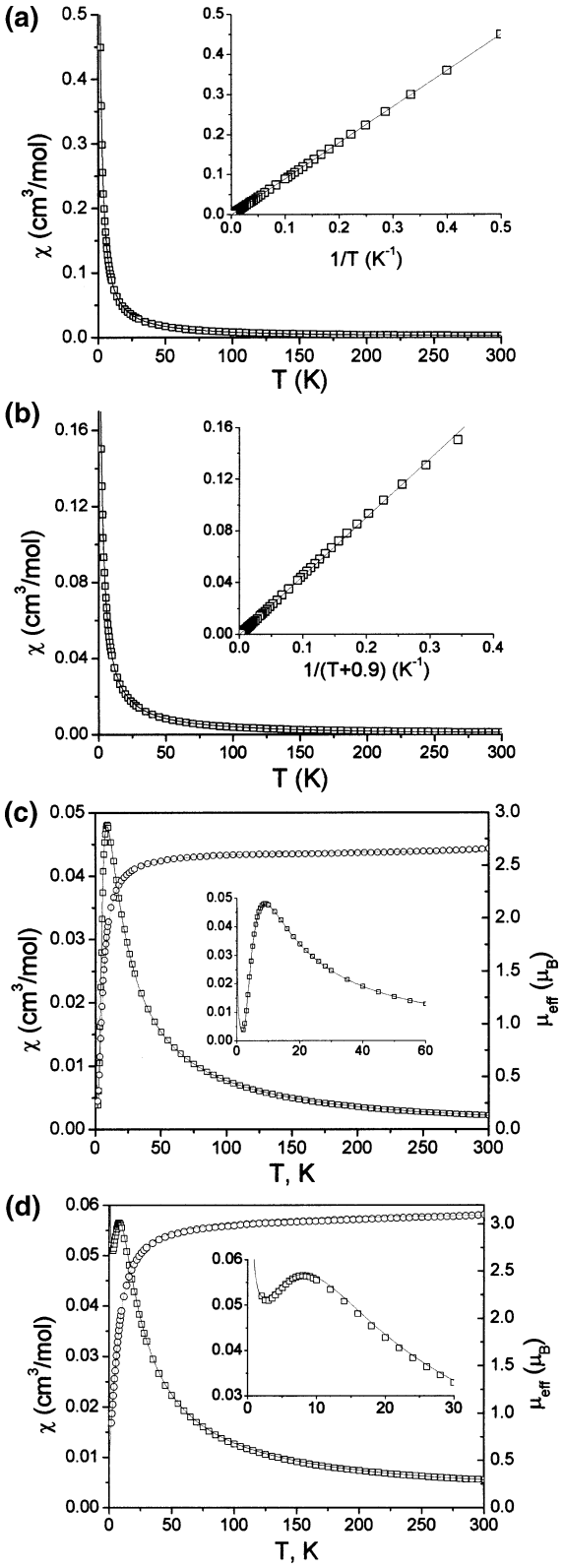

Figure 10. (a) Dependence of the magnetic susceptibility of **5**·4H_2O on temperature. The inset shows the χ dependence on 1/*T*. The lines drawn through the data are the fits to the Curie law. (b) The dependence of magnetic susceptibility of **3**·2H_2O on temperature. The inset shows the χ dependence on 1/*T*. The lines drawn through the data are the fits to the Curie law. (c) The dependence of the magnetic susceptibility and effective moment of **7** on temperature. The line drawn through the data is the fit of eq 3. (d) The dependence of the magnetic susceptibility and effective moment of **1** on temperature. The lines drawn through the data are the fits to eq 4.

ing solids is a common phenomenon.[44] The relatively high temperature of dehydration for **1** reflects the presence of all water molecules as coordinated aqua ligands, rather than as waters of crystallization.[45]

The decomposition profiles for **2**−**7** are similar to those of **1** in the 350−450 °C region but additionally exhibit dehydration processes in the 120−180 °C region attributed to loss of water of crystallization. The thermogravimetric curve for **3**·2H_2O is typical of these materials. The dehydration process at 120−180 °C corresponds to the loss of two water molecules of crystallization. After a plateau from ca. 180 °C to 340 °C, there is a further weight loss of ca. 35%, attributed to decomposition of the organic components, loss of coordinated aqua groups and sublimation of As_2O_3 (35.9%, calculated).

Compounds **8** and **9** exhibit similar profiles to those of **2**−**7** except that the water of crystallization is lost at lower temperatures, ca. 30−70 °C. The lower temperature range for this dehydration process relative to that observed for **2**−**7** reflects the considerably more open structure associated with these molecular species in comparison to the extended structures of **2**−**7**. The rapid weight loss between 380 and 440 °C of ca. 37% is attributed to decomposition of the organic components and loss of As_2O_3 (38.0%, calculated).

Conclusions

Hydrothermal synthesis provides a facile route to novel molecular and one- and two-dimensional organic−inorganic hybrid materials of the copper−organoimine/molybdoarsonate family. As anticipated, the $\{Mo_6O_{18}(O_3AsR)_2\}^{4-}$ cluster provides a structural building block in the structures of the majority of the extended structures, **1** and **3**−**7**. However, the unusual tetranuclear core of **2** illustrates the profound structural consequences of changes in the identity of the ligand to the secondary metal (Cu) on the oxide microstructure.

It is also noteworthy that the materials of this study require the presence of the secondary metal/ligand coordination complex cation for isolation. This structural component serves not only a space-filling and charge-compensating role but is also intimately involved in structural propagation in one and two dimensions. Consequently, while mononuclear Cu(II) subunits generally tether the molybdoarsonate clusters into one-dimensional chains, the binuclear subunits produced by introducing the tpyprz ligand, $\{Cu_2(tpyprz)\}^{4+}$, provide spatial extension into two dimensions in compounds **3** and **7**. Curiously, the mononuclear $\{Cu(terpy)\}^{2+}$ subunit can also link the $\{Mo_6O_{18}(O_3AsR)_2\}^{4-}$ clusters into a network structure in **6**. This structural variability is attributed in part to the number of potential attachment points on the surface of the molybdoarsonate subunits and to the coordination versatility of the Cu(II) site. This latter point reflects the Jahn−Teller distorted coordination geometry of Cu(II) which

(44) (a) Hsu, K.-F.; Wang, S.-L. *Chem. Mater.* **1999**, *11*, 1876. (b) Hsu, K.-F.; Wang, S. L. *Inorg. Chem.* **1998**, *37*, 3230. (c) Hsu, K.-F.; Wang, S.-L. *Inorg. Chem.* **1997**, *36*, 3049.
(45) Ugalde, M.; Gutierrez-Zorrilla, J. M.; Vitoria, P.; Luque, A.; Wéry, A. S. J.; Roman, P. *Chem. Mater.* **1997**, *9*, 2869.

allows square planar, distorted square pyramidal, and distorted octahedral geometries with variable attachments to aqua and/or oxo ligands.

It has become apparent that the significant structural determinants for this class of materials include the dimensions of the oxide substructure and accessible attachment loci, the identity and geometric preferences of the secondary metal center, and the steric and electronic requirements of the organic components. The influences of the secondary metal center will be addressed in some detail in forthcoming descriptions of the structural chemistry of the corresponding Ni(II)−organoimine/molybdophosphonate system.

Acknowledgment. This work was supported by a grant from the National Science Foundation (CHE-0242153).

Supporting Information Available: Tables of atomic positional parameters, bond lengths, bond angles, anisotropic thermal parameters, and calculated hydrogen bond positions for **1**−**9** in CIF format. This material is available free of charge via the Internet http://pubs.acs.org.

IC030171F